Yu Li
State Key Laboratory of Nonlinear Mechanics (LNM),
Institute of Mechanics,
Chinese Academy of Sciences,
Beijing 100190, China;
School of Engineering Science,
University of Chinese Academy of Sciences,
Beijing 100049, China

Han Fei
Department of Traumatic Orthopedics,
Beijing Jishuitan Hospital,
Beijing 100035, China

Jun Wang
State Key Laboratory of Nonlinear Mechanics (LNM),
Institute of Mechanics,
Chinese Academy of Sciences,
Beijing 100190, China;
School of Engineering Science,
University of Chinese Academy of Sciences,
Beijing 100049, China

Ting Li
Department of Traumatic Orthopedics,
Beijing Jishuitan Hospital,
Beijing 100035, China

Yihui Feng[1]
State Key Laboratory of Nonlinear Mechanics (LNM),
Institute of Mechanics,
Chinese Academy of Sciences,
Beijing 100190, China
e-mail: fengyh@lnm.imech.ac.cn

Yong Huan[1]
State Key Laboratory of Nonlinear Mechanics (LNM),
Institute of Mechanics,
Chinese Academy of Sciences,
Beijing 100190, China;
School of Engineering Science,
University of Chinese Academy of Sciences,
Beijing 100049, China;
Beijing Key Laboratory of Engineered Construction and Mechanobiology,
Institute of Mechanics,
Chinese Academy of Sciences,
Beijing 100190, China
e-mail: huany@lnm.imech.ac.cn

The Regularity of Stress Shielding in Internal Fixation Characterized by Hydromechanics

Stress shielding is an important factor in the internal fixation of a fracture. To explore the regularity of stress shielding in internal fixation, a simplified model of a comminuted femoral shaft fracture bridged by a locking plate was established and finite element analysis was performed to analyze the load distribution between the plate and femur from the proximal end of the femur to the fracture line and investigate the stress shielding degree of the plate on the bone. The stress, deformation, and axial compressive force distribution of four internal fixation schemes under compression were obtained, and the stress shielding degrees on each section was calculated. To compare the regularity of stress shielding and flow distribution, the relationship between the compressive force increment and stress shielding degree was established. The normalized curves of compressive force increment with the plate section position were compared with the flow distribution in a Z-type manifold, a parallel pipe system similar to an internal fixation system in structure and working characteristics. For quantitative comparison, the similarity between normalized curves of the compressive force increment and simulated flow distribution was calculated. The regularity of load distribution along the section position of the plate was similar to the flow distribution in the Z-type manifold. Therefore, the flow distribution pattern of the Z-type manifold can be used to characterize the regularity of load distribution in internal fixation. This study provided a new method to characterize the stress shielding degree of a locking plate on bone. [DOI: 10.1115/1.4052884]

Keywords: internal fixation of fracture, stress shielding, characterization method, flow distribution of Z-type manifold

1 Introduction

Stress shielding refers to the reduction of bone stress caused by an implant, which affects the normal growth of bone. In 1884, Wolff proposed that bone grows where needed and absorbs where not needed, in what became known as Wolff's law. The bone plates used to treat fractures have a much higher stiffness than cortical bone, and bone–implant coupling structures are often statically indeterminate; thus, the bone plates carry more body load and create stress shielding. Researchers have known for decades that stress shielding, as a long-term effect, may interfere with bone healing and potentially cause considerable bone loss underneath the plate [1–3]. In the internal fixation system of bone plates, stress shielding is considered the main reason leading to its failure. McKibbin [4] showed that a callus is initially formed in the early stage of healing, and the stress shielding of the plate on the femoral shaft fracture space is conducive to the early healing of the fracture. However, for the bone underneath the plate, stress

[1]Corresponding authors.

Manuscript received July 14, 2021; final manuscript received October 24, 2021; published online December 17, 2021. Assoc. Editor: Joseph Wallace.

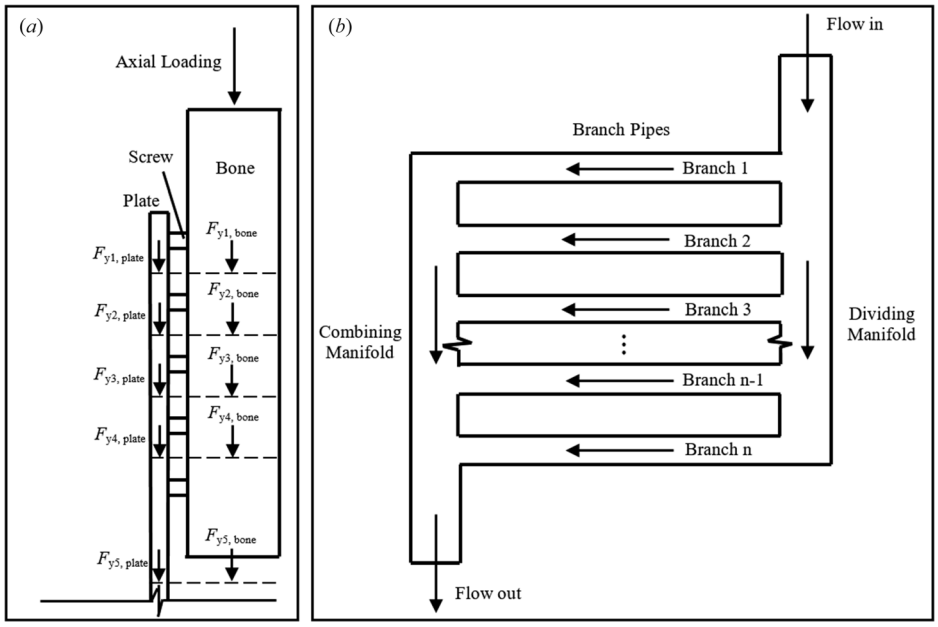

Fig. 1 (*a*) Bone–screw–plate coupling structure versus the (*b*) Z-type manifold

shielding caused the reduction of bone load, which would lead to bone loss and further osteoporosis [5]. Consequently, it is important to ensure appropriate stress shielding in the design of internal fixation [6].

Many earlier studies have analyzed the stress shielding degree of the bone–implant coupling structure. Some researchers used stress change to represent the degree of stress shielding. Ramakrishna et al. [7,8] extracted the normal stress on the bone cross section along the length of a bone–plate interface, explored the influence of different materials or lengths of plates and the number of screws or location on the stress shielding degree, and proposed that modulus variation in plates did offer less stress-shielding but not significant enough as the dependency of stress-shielding was more on the geometry of the plate, number and placement of screws. Fouad et al. [1,9,10] evaluated the stress shielding degree by comparing von Mises stress at the same position when different bone plates were used. Additionally, some scholars expressed the stress shielding degree by defining characterization parameters. Zhou et al. [11,12] used the ratio of stress on the same position of the bone with or without internal fixation to characterize the stress shielding rate, and they analyzed the stress shielding degree in the internal fixation of tibia comminuted fractures with different bone plates. Gefen et al. [13] used a stress transfer parametric approach to quantify the screw–bone load transfer, and Haase et al. [14] defined a strain energy density transfer parameter to represent the strain energy density transfer between screws and bone. The regularity of stress shielding in the bone–implant coupling structure is an important problem in the study of bone biomechanics.

The bone–screw–plate structure is a common structure that causes stress shielding and it was used as an example to explore the regularity of stress shielding. A simplified model of internal fixation for a comminuted fracture is shown in Fig. 1(*a*). The model is structurally very similar to a Z-type manifold. A Z-type manifold is a type of parallel pipe system mainly composed of a dividing manifold, a combining manifold, and parallel branch pipes of identical dimensions. In addition, the distribution of load or flow is their common working characteristic [15–17]. The applied load is divided into the load on the bone and the load on the plate, and the sum of compressive forces remain constant on each section. In the Z-type manifold, the fluid flows into the dividing manifold and the combining manifold, as shown in Fig. 1(*b*). The sum of flow on each section is also unchanged and equal to the total input flow. In this study, the similarities between the "load distribution" in the internal fixation system and the "flow distribution" in the Z-type manifold were investigated.

A simplified model of a comminuted femoral shaft fracture bridged by a locking plate was used to analyze the stress shielding degree of the plate on the bone along the longitudinal direction of the femur in different screw distribution schemes. The load distribution in the bone–screw–plate coupling structure and the branch flow distribution of the Z-type manifold were compared to verify the consistency of these two regularities.

2 Method

2.1 Geometric Model. In this paper, a simplified model of a femoral shaft comminuted fracture bridged by a locking plate was used as an example to explore the stress shielding regularity of a plate on bone. The distal and proximal femur has little influence on the stress of the plate or bone underneath the plate, and the shape of the femoral shaft was similar to a hollow cylinder. Therefore, the half femoral shaft was simplified into a hollow cylinder with an outer diameter of 25 mm, an inner diameter of 12 mm, and a length of 150 mm, which is consistent with the adult example used in the finite element model [18,19]. The screw was simplified into a cylinder with a diameter of 4.5 mm and the locking plate was simplified into a plate-like model. According to the use rules of the locking compression plate [20], a simplified model of the 10-hole plate was used with a length of 189 mm, a width of 15 mm, and screw hole diameter of 4.5 mm. The focus of this study was the overall distribution of stress and force on cross sections, rather than the stress concentration. The details of the structure shape mainly affect the local stress, with little effect on the overall distribution of stress and forces. Therefore, the simplification of the model shape did not affect the conclusion of this study. The above models were established in three-dimensional modeling software (SOLIDWORKS, Waltham, MA).

The bones, screws, and plate were assembled in SOLIDWORKS. The space between two half bones was set to 5 mm to simulate the comminuted fracture space. The gap between the plate and bone was 2 mm, in line with the use rules of the locking plate. In this paper, four schemes of screw distribution were used as examples to analyze stress shielding. The screws were distributed symmetrically along the fracture line and the spacing between adjacent

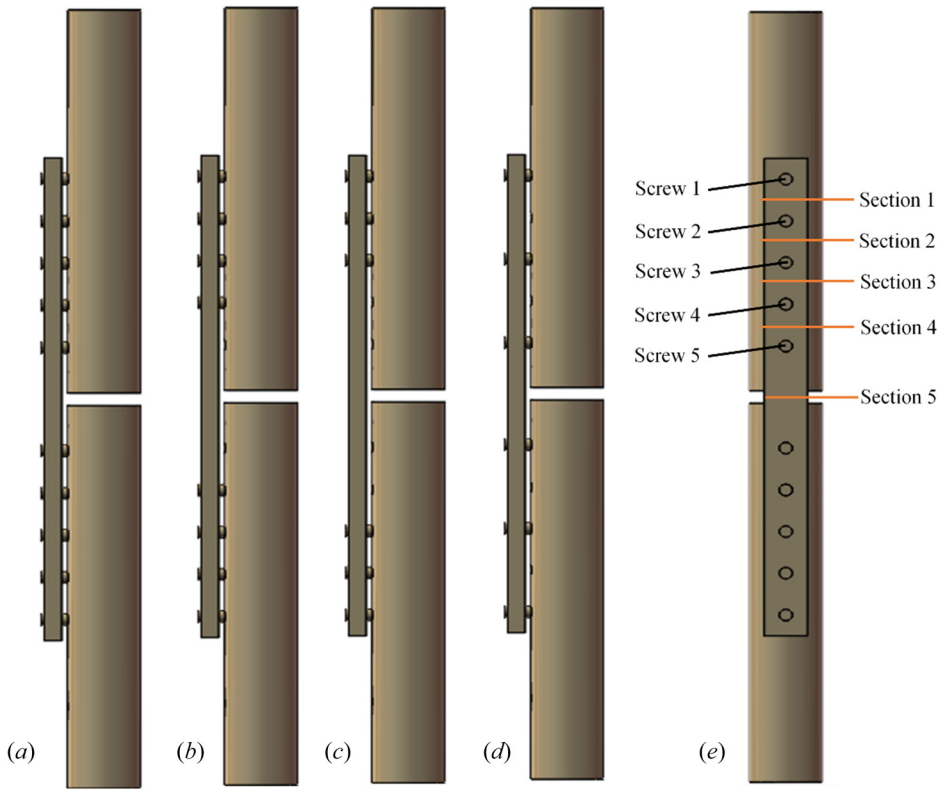

Fig. 2 Screw distribution: (*a*) scheme 1, (*b*) scheme 2, (*c*) scheme 3, (*d*) scheme 4, and (*e*) designation of screws and sections

screws was constant. The position and designation of screws and sections are shown in Fig. 2.

2.2 Finite Element Model. The bone–screw–plate assembly models mentioned have meshed in finite element preprocessing software (Altair HyperMesh, Troy, MI). The mesh type was tetrahedral, and the mesh numbers of bones, screws, and plates were 231,216, 123,217, and 73,554, respectively. The mesh models were imported into finite element analysis software (ABAQUS, Waltham, MA) for simulation. The simplified bones, screws, and plates were treated as continuous, homogeneous, and isotropic linear elastic materials [21]. The femoral shaft was cortical bone; as a result, Young's modulus of the simplified femoral shaft was set to 16.8 GPa and the Poisson's ratio was 0.3. The implant materials were set as a titanium alloy with Young's modulus of 110 GPa and a Poisson's ratio of 0.3 [22]. Considering the function of the locking screw, the screws were bound to the bones and plate.

The realistic mode of loading in a femur is complex; however, the axial compressive load is more prominent in long bones [5]. This study focused on the axial compressive load. Therefore, the load was simplified to pure compression. An adult weighing 100 kg, standing on two legs was used as an example, and the axial compressive force of 500 N was applied to the cross section of the simplified proximal femur [18,19,22]. The bottom surface of the simplified distal femur was fixed as the boundary condition of the bone–screw–plate coupling structure. The loading regime and boundary condition are shown in Fig. 3. Bending of the structure because of plate eccentricity was allowed.

2.3 Research Method. The finite element (FE) stress maps and displacement maps of the four schemes were obtained and the rationality of the finite element simulation was verified by analyzing its consistency with the literature. The values of axial compressive force on each section of bone and plate were extracted to calculate the stress shielding degree of four schemes and axial compressive force increment on each section of the plate. The relationship between the plate axial compressive force increment and stress shielding degree in each section was established to build a bridge between the stress shielding degree and branch flow distribution in the Z-type manifold. Furthermore, the curve of the

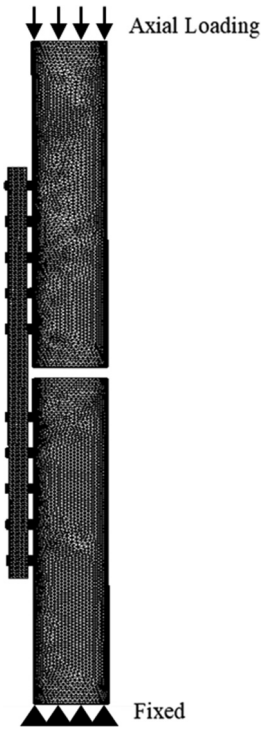

Fig. 3 Loading regime and boundary condition

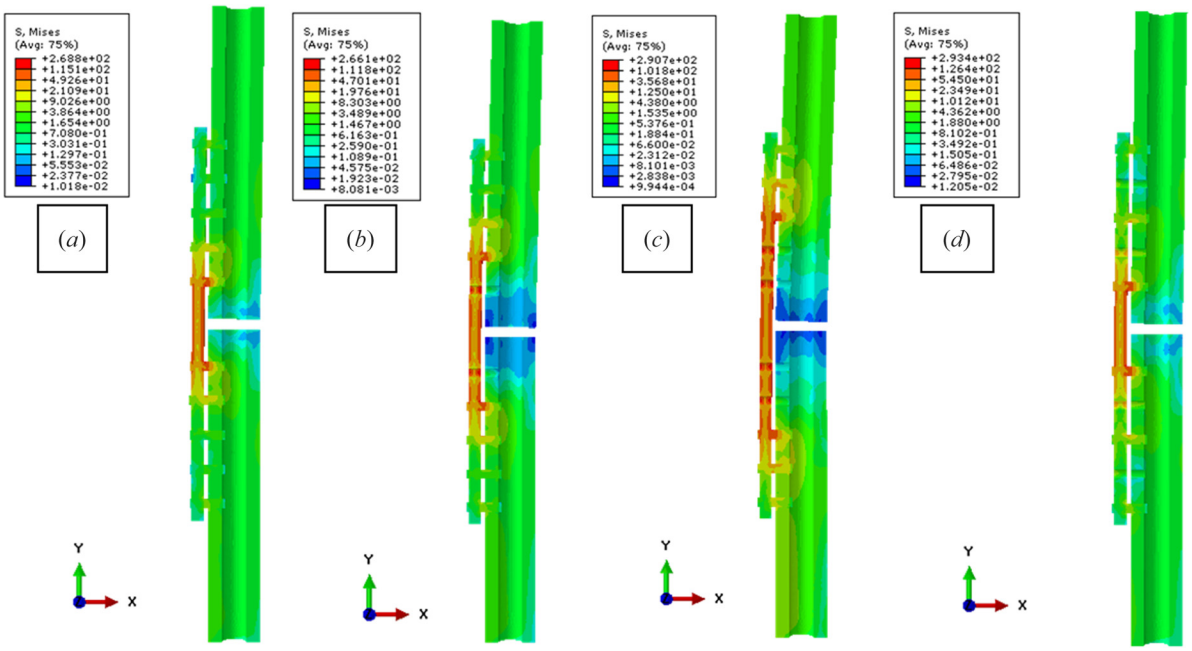

Fig. 4 FE stress maps of the bone–screw–plate coupling structure in (*a*) scheme 1, (*b*) scheme 2, (*c*) scheme 3, and (*d*) Scheme 4

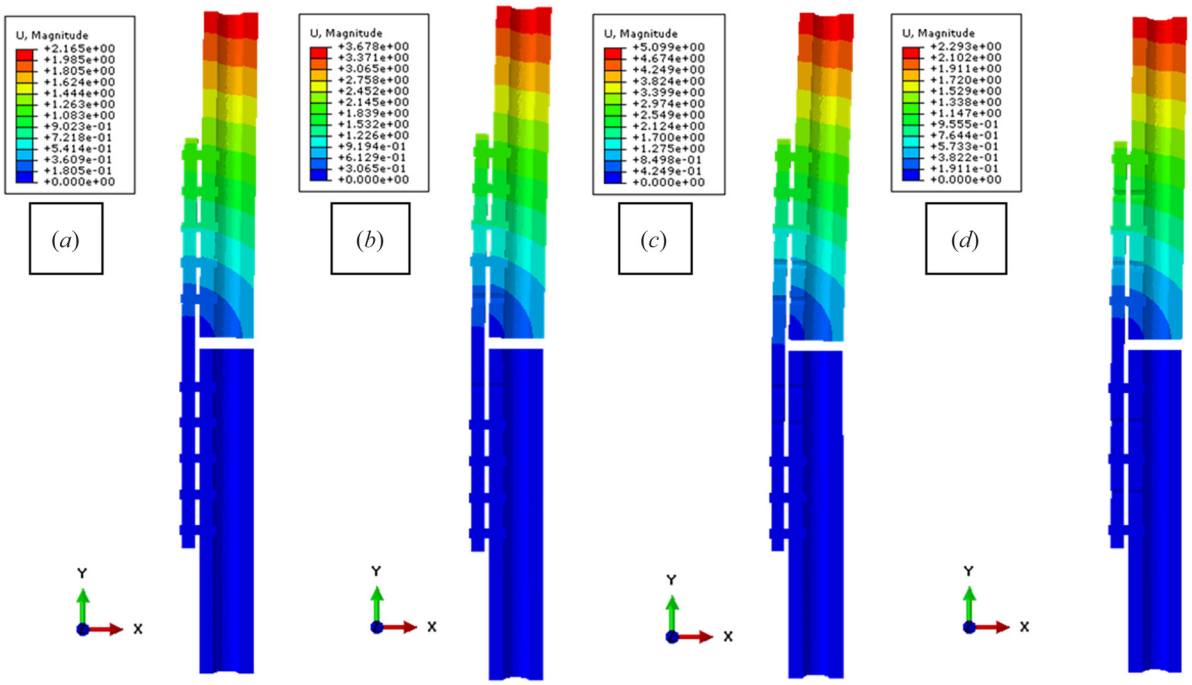

Fig. 5 FE displacement maps of the bone–screw–plate coupling structure in (*a*) scheme 1, (*b*) scheme 2, (*c*) scheme 3, and (*d*) scheme 4

plate axial compressive force increment with the section position in scheme 1 and the curves of the branch flow distribution in the Z-type manifold in literature was normalized and compared.

3 Results

3.1 The Stress Shielding Degree of a Plate on Bone With Four Distributions of Screws. The FE stress maps of the bone–screw–plate coupling structure in four schemes are shown in Fig. 4 and the FE displacement maps are shown in Fig. 5.

As shown in Figs. 4(*a*), 4(*b*), and 4(*c*), the reduction of the screw number near the fracture causes the working length of the plate, high-stress area of the plate, and low-stress area of bone to increase. Moreover, as shown in Figs. 5(*a*), 5(*b*), and 5(*c*) the reduction of screw number near the fracture causes the deformation of the bone–screw–plate coupling structure to increase.

As shown in Figs. 4(*c*) and 4(*d*), with the same number of screws, the working length, high-stress area of the plate, and low-stress area of the bone were smaller when the screws were dispersed than when the screws were concentrated away from the

Table 1 Distribution of the axial compressive force of the plate and bone, and stress shielding degree on each section

Section number		1	2	3	4	5
Scheme 1	$F_{y1,\text{plate}}$ (N)	−44.34	−62.02	−55.71	−76.23	−499.90
	$F_{y1,\text{bone}}$ (N)	−455.50	−437.50	−445.20	−425.10	0.00
	Stress shielding degree (%)	8.87	12.42	11.12	15.21	100
Scheme 2	$F_{y2,\text{plate}}$ (N)	−43.39	−47.95	−87.54	−506.00	−499.6
	$F_{y2,\text{bone}}$ (N)	−456.30	−451.50	−426.00	0.66	0.00
	Stress shielding degree (%)	8.68	9.60	17.05	100.13	100
Scheme 3	$F_{y3,\text{plate}}$ (N)	−27.29	−68.01	−537.80	−508.70	−499.30
	$F_{y3,\text{bone}}$ (N)	−472.40	−431.20	0.14	0.08	0.00
	Stress shielding degree (%)	5.46	13.62	100	100.02	100
Scheme 4	$F_{y4,\text{plate}}$ (N)	−65.60	−66.21	−34.60	−36.22	−499.90
	$F_{y4,\text{bone}}$ (N)	−434.30	−433.50	−466.90	−466.80	0.00
	Stress shielding degree (%)	13.12	13.25	6.90	7.20	100

fracture. As shown in Figs. 5(*c*) and 5(*d*), the dispersed screws reduce the deformation of the bone–screw–plate coupling structure.

Because the axial compressive load is more prominent in the long bones [5], and this paper focuses on the overall influence of stress shielding, the distribution of axial compressive force between the bone and plate on the same section is selected as the evaluation index of the stress shielding degree, rather than the stress value at a certain point or several points.

The stress shielding degree was defined as Eq. (1)

$$\beta_i = \frac{F_{yi,\text{plate}}}{F_{yi,\text{plate}} + F_{yi,\text{bone}}} \tag{1}$$

i is the section position, $F_{yi,\text{plate}}$ is the axial compressive force on section i of the plate, and $F_{yi,\text{bone}}$ is the axial compressive force on Section i of the bone. To avoid the effect of stress concentration near the screw holes, the axial compressive force on the bisection section between the adjacent screw holes of the bone and plate was extracted.

As shown in Fig. 1(*a*), the total axial compressive load is divided into the forces on the bone and plate on each section, $F_{yi,\text{plate}}$ and $F_{yi,\text{bone}}$. $F_{yi,\text{plate}}$ and $F_{yi,\text{bone}}$ are, respectively, the integrals of the axial compressive stress of plate and bone on each section in ABAQUS and are shown in Table 1. The stress shielding degrees of the plate on the bone in four schemes were calculated by Eq. (1), and are shown in Table 1 and Fig. 6. The stress shielding degree of scheme 3 reached about 100% at Sec. 3, scheme 2 reached 100% at Sec. 4, while schemes 1 and 4 reached 100% at Sec. 5. In addition, the stress shielding degree of scheme 1 was greater than scheme 4 after Sec. 2. Therefore, scheme 3 had the most stress shielding, followed by schemes 2, 1, and 4 had the least degree of stress shielding.

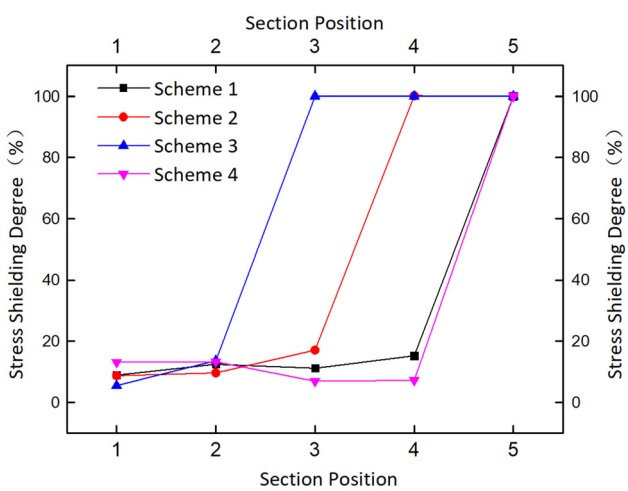

Fig. 6 The stress shielding regularity of the plate on bone in four schemes

3.2 Comparison of the Load Increment-Section Position Curve of the Plate After Crossing Screws and the Flow Distribution-Branch Position Curve of the Z-Type Manifold. To further establish the relationship between the stress shielding degree and branch flow distribution in the Z-type manifold, the stress shielding degree was reflected by the axial compressive force increment Δ_i, which referred to the axial compressive force on section i minus the axial compressive force on section $i-1$ of the plate. The relationship between them is shown in the following equation:

$$\beta_i = \frac{\sum_{x=1}^{i} \Delta_i}{F_{yi,\text{plate}} + F_{yi,\text{bone}}} \tag{2}$$

i is the section position, $F_{yi,\text{plate}}$ is the axial compressive force on Section i of the plate, $F_{yi,\text{bone}}$ is the axial compressive force on section i of the bone, and Δ_i is the compressive force increment on section i of the plate.

The curves of the plate axial compressive force increment with the section position in scheme 1 and the theoretical value [23], simulated value [24], and experimental value [25] of the branch flow distribution in the Z-type manifold were normalized. The branch pipe names before normalization are shown in Fig. 1(*b*). The deviation normalization was used to map the data to the 0–1 range, as shown in the following equation:

$$X^* = \frac{X - X_{\min}}{X_{\max} - X_{\min}} \tag{3}$$

X^* is the value after normalization, X is the value before normalization, and $X_{\max}$ and $X_{\min}$ are the maximum and minimum values in a dataset, respectively.

As shown in Fig. 7(*a*), along the simplified proximal femur to the fracture gap, the axial compressive force increment of the plate significantly increases after a slight decrease. This is very similar to the normalized curve of the flow distribution simulated values with branch position in the Z-type manifold. In addition, there was a good match between these two curves. For quantitative comparison, the similarity S between the flow distribution simulated value [24] and axial compressive force increment normalized curve was defined as Eq. (4). The similarity S curve is shown in Fig. 7(*b*)

$$S = \left(1 - \frac{|y_{\text{flow}} - y_{\text{force}}|}{y_{\text{full}}}\right) \times 100\% \tag{4}$$

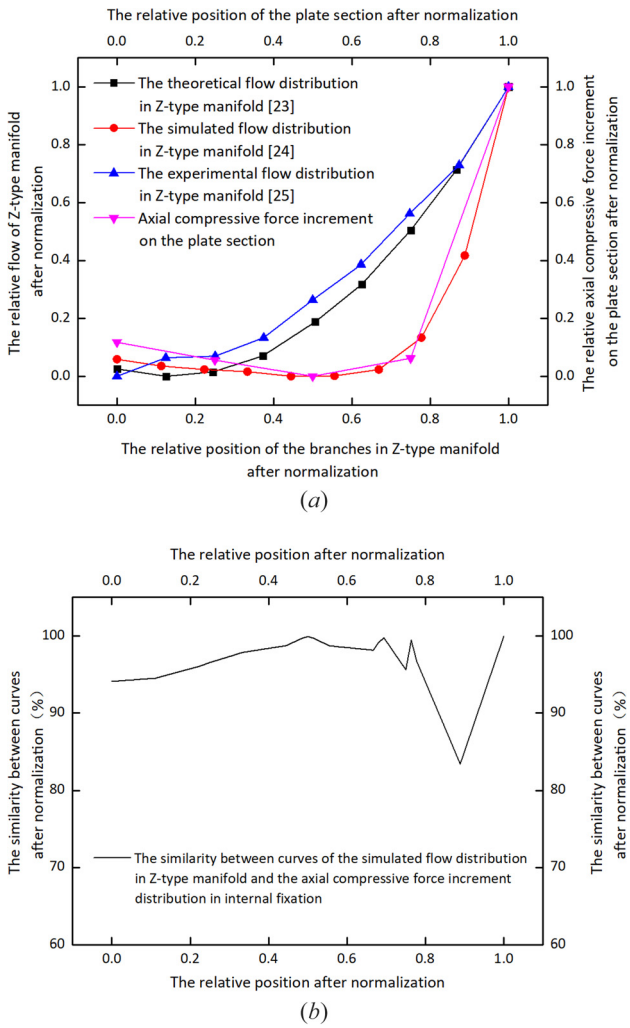

Fig. 7 (*a*) Comparison of axial compressive force increment with the section position of the plate and flow distribution in the Z-type manifold. (*b*) The similarity between curves of the simulated flow distribution in the Z-type manifold and axial compressive force increment distribution in the internal fixation.

y_{flow} is the simulated value [24] of the branch flow distribution in the Z-type manifold after normalization, y_{force} is the axial compressive force increment of the plate after normalization, and y_{full} is the full scale value after normalization.

Statistically, the similarity between the two curves was greater than 83% in the full range, with more than 90% of the range reaching more than 90% similarity. Because the results in this paper were obtained through simulation, they have a good agreement with the simulation values of the branch flow distribution and less agreement with the theoretical and experimental values. However, as shown in Fig. 7(*a*), the curves of the theoretical, experimental, and axial compressive force increment all start with low values and little change, increasing significantly in the posterior sections.

4 Discussion

This study analyzed the stress, deformation, and axial compressive force distribution of a bone–screw–plate coupling structure under four internal fixation schemes. The results show that the reduction of screw number near the fracture causes the working length of the plate, high-stress area of the plate, and stress shielding degree to increase. Therefore, there is an increased potential for plate damage and osteoporosis because of low stress in healthy bone. At the same time, the deformation of the bone–screw–plate coupling structure also obviously increased, which means that the stability of the structure was greatly reduced.

With the same number of screws, the working length, high-stress area of the plate, and stress shielding degree were less when the screws were dispersed than when the screws were concentrated away from the fracture. Therefore, the potential for plate damage and osteoporosis in the healthy bone was reduced. At the same time, dispersed screws reduced the deformation of the bone–screw–plate coupling structure, which means the stability of the structure was increased.

Scheme 4 achieved the best results among the four tested schemes, which is consistent with the results of Stoffel et al. [26] and Ramakrishna et al. [7]. The number of screws has a significant effect on stability: the more screws close to the fracture space, the higher the compression stability, significantly reducing the stress shielding area. This proves that the finite element simulation in this paper is reasonable.

With the fracture line as the axis of symmetry, the structural characteristics and stress distribution of the bone–screw–plate coupling structure were basically symmetrical. Therefore, the structure from the simplified proximal femur to the half of the fracture space was selected for comparison with the Z-type manifold.

Stress shielding is caused by uneven load distribution between the bone and plate. The stress shielding regularity is essentially the force distribution regularity. One of the characteristics of the Z-type manifold is the flow distribution. The regularity of the distribution is a common characteristic that creates a relationship. Additionally, the model of the internal fixation system and Z-type manifold were very similar in structural and working characteristics. Therefore, the uneven distribution in the two systems was compared.

To explore whether the "load distribution" in the bone–screw–plate coupling structure and "flow distribution" in the Z-type manifold have the same regularity, the normalized curve of the axial compressive force increment with the plate section position was obtained and compared with the normalized flow distribution curves of the Z-type manifold in literature. The regularities, which all start with low values and little changes, increasing significantly in the posterior sections, were similar. Furthermore, the agreement between the simulated curves of the branch flow distribution and axial compressive force was high. The principle of this phenomenon maybe because of some commonalities in the distribution characteristics. The resultant axial compressive force of the bone and plate on each section is constant and equal to the total force applied. The total flow of the dividing manifold and combining manifold on each section is also unchanged, equal to the total input flow. The invariable total amount is a common characteristic. Moreover, the axial compressive force increment on each plate section influences each other, and their sum is the total force applied. The flow values of each branch of the Z-type manifold also affect each other, and their sum is equal to the total flow of the input. The interaction between subunits is another common feature. Because the stress shielding degree is expressed in terms of the compressive force increment as in Eq. (2), the similarity between the compressive force increment and branch flow distribution allows us to establish the relationship between the stress shielding regularity and branch flow distribution.

As shown in Figs. 6 and 7(*a*), the stress shielding degree far from the fracture line increases slowly, while that close to the fracture line increases quickly. Therefore, the bone near the fracture line is at greater risk of osteoporosis. In addition, as shown in the "scheme 3" and "scheme 4" curves in Fig. 6 with the same number of screws, the stress shielding degree of scheme 3 is greater than that of scheme 4. This proves that increasing the number of screws near the fracture line is more effective than screws farther away in reducing stress shielding.

Based on the similarity between the load distribution in the internal fixation system and the flow distribution in the Z-type manifold, it was proposed that the regularity of the stress shielding degree in internal fixation can be characterized by the flow

distribution regularity in the Z-type manifold. Similar studies [1,7–14] explored the regularity of stress shielding by evaluating the degree of stress shielding using parameters in the internal fixation structure itself, such as normal stress, von Mises stress, stress ratio, and strain energy density. This perspective provides a new way to characterize stress shielding.

However, there are still some limitations in this study. This study only explored stress shielding under axial compressive load; however, the actual load conditions are more complex. Additionally, it is not clear that the change in a similarity between the flow distribution in the Z-type manifold and the axial compressive force distribution in the internal fixation system after changing their geometric sizes. The corresponding changes with the changing parameters of the two models, such as the number and spacing of branches and screws, have also not been explored. These gaps are expected to be investigated in future studies.

5 Conclusion

A simplified model of a comminuted femoral shaft fracture bridged with a locking plate was established. The load and deformation distributions of the bone–screw–plate coupling structure under pure compression in four screw distribution schemes were observed by finite element analysis. The degree of stress shielding was expressed by the load distribution and there were similarities between the load distribution and flow distribution of the Z-type manifold. This study determined that the regularity of the load distribution between the plate and bone in the internal fixation system can be characterized by the flow distribution regularity in the Z-type manifold. Increasing the number of screws near the fracture line more effectively reduces stress shielding than screws farther away. This provides a new method for characterizing the stress shielding of a plate on bone.

Funding Data

- National Natural Science Foundation of China (Grant No. 11972037; Funder ID: 10.13039/501100001809).

References

[1] Bagheri, Z. S., Avval, P. T., Bougherara, H., Aziz, M., Schemitsch, E. H., and Zdero, R., 2014, "Biomechanical Analysis of a New Carbon Fiber/Flax/Epoxy Bone Fracture Plate Shows Less Stress Shielding Compared to a Standard Clinical Metal Plate," ASME J. Biomech. Eng., **136**(9), p. 091002.

[2] Zhao, X., Jing, W., Yun, Z., Tong, X., Li, Z., Yu, J., Zhang, Y., Zhang, Y., Wang, Z., Wen, Y., Cai, H., Wang, J., Ma, B., and Zhao, H., and, 2021, "An Experimental Study on Stress-Shielding Effects of Locked Compression Plates in Fixing Intact Dog Femur," J. Orthop. Surg. Res., **16**(1), p. 97.

[3] Uhthoff, H. K., Poitras, P., and Backman, D. S., 2006, "Internal Plate Fixation of Fractures: Short History and Recent Developments," J. Orthop. Sci., **11**(2), pp. 118–126.

[4] Mckibbin, B., 1978, "The Biology of Fracture Healing in Long Bones," J. Bone Jt. Surg.-Br., **60-B**(2), pp. 150–162.

[5] Ramakrishna, K., Sridhar, I., Sivashanker, S., Khong, K. S., and Ghista, D. N., 2004, "Design of Fracture Fixation Plate for Necessary and Sufficient Bone Stress Shielding," JSME Int. J. Ser. C-Mech. Syst. Mach. Elem. Manuf., **47**(4), pp. 1086–1094.

[6] Goel, V. K., Lim, T. H., Gwon, J., Chen, J. Y., Winterbottom, J. M., Park, J. B., Weinstein J. N., and Ahn, J. Y., 1991, "Effects of Rigidity of an Internal Fixation Device a Comprehensive Biomechanical Investigation," Spine, **16**(3), pp. S155–S161.

[7] Ramakrishna, K., Sridhar, I., Sivashanker, S., Ganesh, V. K., and Ghista, D. N., 2005, "Analysis of an Internal Fixation of a Long Bone Fracture," J. Mech. Med. Biol., **05**(01), pp. 89–103.

[8] Ganesh, V. K., Ramakrishna, K., and Ghista, D. N., 2005, "Biomechanics of Bone-Fracture Fixation by Stiffness-Graded Plates in Comparison With Stainless-Steel Plates," Biomed. Eng. Online, **4**(1), pp. 1–15.

[9] Fouad, H., 2011, "Assessment of Function-Graded Materials as Fracture Fixation Bone-Plates Under Combined Loading Conditions Using Finite Element Modelling," Med. Eng. Phys., **33**(4), pp. 456–463.

[10] Fice, J., and Chandrashekar, N., 2012, "Tapered Fracture Fixation Plate Reduces Bone Stress Shielding: A Computational Study," J. Mech. Med. Biol., **12**(04), p. 1250072.

[11] Zhou, K., and Yang, H., 2020, "Effects of Bone-Plate Material on the Predicted Stresses in the Tibial Shaft Comminuted Fractures: A Finite Element Analysis," J. Mech. Med. Biol., **12**(4), pp. 1–9.

[12] Piao, C., Wu, D., Min, L., and Ma, H., 2014, "Stress Shielding Effects of Two Prosthetic Groups After Total Hip Joint Simulation Replacement," J. Orthop. Surg. Res., **9**(1), pp. 1–8.

[13] Gefen, A., 2002, "Computational Simulations of Stress Shielding and Sone Resorption Around Existing and Computer-Designed Orthopaedic Screws," Med. Biol. Eng. Comput., **40**(3), pp. 311–322.

[14] Haase, K., and Rouhi, G., 2013, "Prediction of Stress Shielding Around an Orthopedic Screw: Using Stress and Strain Energy Density as Mechanical Stimuli," Comput. Biol. Med., **43**(11), pp. 1748–1757.

[15] Saidpour, S. H., 2006, "Assessment of Carbon Fibre Composite Fracture Fixation Plate Using Finite Element Analysis," Ann. Biomed. Eng., **34**(7), pp. 1157–1163.

[16] Pigford, R. L., Ashraf, M., and Miron, Y. D., 1983, "Flow Distribution in Piping Manifolds," Ind. Eng. Chem. Fundam., **22**(4), pp. 463–471.

[17] Wang, C. C., Yang, K. S., Tsai, J. S., and Chen, I. Y., 2011, "Characteristics of Flow Distribution in Compact Parallel Flow Heat Exchangers, Part II: Modified Inlet Header," Appl. Therm. Eng., **31**(16), pp. 3235–3242.

[18] Fouda, N., Mostafa, R., and Saker, A., 2019, "Numerical Study of Stress Shielding Reduction at Fractured Bone Using Metallic and Composite Bone-Plate Models," Ain Shams Eng. J., **10**(3), pp. 481–488.

[19] Nassiri, M., MacDonald, B., and O'Byrne, J. M., 2013, "Computational Modelling of Long Bone Fractures Fixed With Locking Plates - How Can the Risk of Implant Failure Be Reduced," J. Orthop., **10**(1), pp. 29–37.

[20] Gautier, E., and Sommer, C., 2003, "Guidelines for the Clinical Application of the LCP," Injury-Int. J. Care Injured, **34**(supp-S2), pp. 63–76.

[21] El'Sheikh, H. F., MacDonald, B. J., and Hashmi, M. S. J., 2003, "Finite Element Simulation of the Hip Joint During Stumbling: A Comparison Between Static and Dynamic Loading," J. Mater. Process Technol., **143–144**(supp-S1), pp. 249–255.

[22] Sheng, W., Ji, A., Fang, R., He, G., and Chen, C., 2019, "Finite Element- and Design of Experiment-Derived Optimization of Screw Configurations and a Locking Plate for Internal Fixation System," Comput. Math. Methods Med., **2019**(2), pp. 1–15.

[23] Yang, H., Yuan, D., Hu, H., Jiang, Y., and Tang, D., 2018, "Theoretical and Experimental Research on Flow Distribution of Solar Collector System," J. Eng. Thermophys., **39**(7), pp. 1505–1511.

[24] Siddiqui, O. K., Al-Zahrani, M., Al-Sarkhi, A., and Zubair, S. M., 2020, "Flow Distribution in U- and Z-Type Manifolds: Experimental and Numerical Investigation," Arabian J. Sci. Eng., **45**(7), pp. 6005–6020.

[25] Facao, J., 2015, "Optimization of Flow Distribution in Flat Plate Solar Thermal Collectors With Riser and Header Arrangements," Sol. Energy, **120**, pp. 104–112.

[26] Stoffel, K., Dieter, U., Stachowiak, G., Gachter, A., and Kuster, M. S., 2003, "Biomechanical Testing of the LCP - How Can Stability in Locked Internal Fixators Be Controlled," Injury-Int. J. Care Injured, **34**(supp-S2), pp. 11–19.